THE JOURNAL OF PHYSICAL CHEMISTRY A
A JOURNAL OF THE AMERICAN CHEMICAL SOCIETY

pubs.acs.org/JPCA

Article

Charge-Shifted Weak Noncovalent Interactions in the Atmospherically Important OCS Microhydrates

Published as part of The Journal of Physical Chemistry virtual special issue "Early-Career and Emerging Researchers in Physical Chemistry Volume 2".

Saptarsi Mondal*

Cite This: https://doi.org/10.1021/acs.jpca.2c07670

Read Online

ACCESS | Metrics & More | Article Recommendations | Supporting Information

ABSTRACT: Stratospheric aerosol, mainly comprising microhydrated carbonyl sulfide (OCS), is among the primary drivers of climate change. In this study, we investigate the effect of microhydration on the structure, energetics, and vibrational properties of the neutral OCS molecule using ab initio calculation, molecular electrostatic potential (MESP), topological analyses of electron density, and natural bond orbital (NBO) analyses. The complexation energy increases with the cluster size, and the first solvation shell of OCS consists of four water molecules that interact with the OCS moiety preferentially through $S_{OCS}\cdots O_W$, $O_{OCS}\cdots O_W$, and $C_{OCS}\cdots O_W$ type of weak noncovalent interaction instead of the typical $O_{OCS}\cdots H-O_W$ and $S_{OCS}\cdots H-O_W$ H-bonds. These noncovalent interactions originate due to the electron shift from the water oxygen lone pair to the antibonding orbital of C═S [BD*(C═S)], sometimes via BD*(C═O), which substantially perturbs the bending mode of surrounding water molecules. The present study thus unravels the underlying relationship between the OCS atmospheric hydrolysis and the charge-shifted noncovalent interactions.

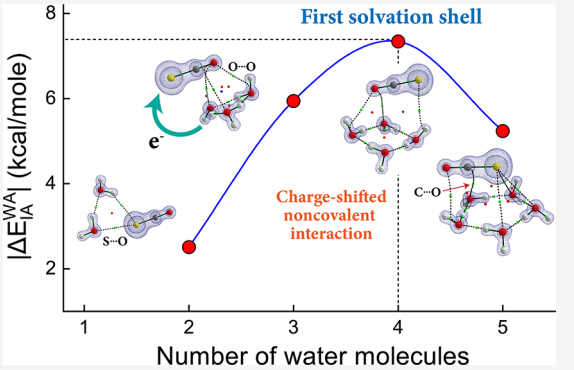

1. INTRODUCTION

The most abundant and stable sulfur-containing gas is carbonyl sulfide (OCS), which maintains the global sulfur cycle. Being one of the primary greenhouse gases involved in stratospheric aerosol formation, OCS substantially affects the earth's radiation balance and is one of the main drivers of climate change.[1−6] Therefore, understanding the properties and behavior of OCS is crucial to realizing its impact on climate change.[7,8] Numerous studies have been conducted to understand the source and the sink of OCS promoting aerosol formation in the stratosphere.[1,2,4] The existence of other S-containing species and their water clusters in the stratosphere were observed both theoretically and experimentally.[4,7,9,10] In fact, water was shown to catalyze the hydrolysis reaction of the S-containing compounds.[11,12] It was observed that the atmospheric hydrolysis of OCS is the most efficient pathway among other physicochemical processes through which S-containing compounds get removed from the atmosphere.[7,11] The atmospheric hydrolysis depends on the relative humidity and water content, suggesting that the water hydration structure plays a pivotal role in the process.[4,7,9,11] Therefore, a detailed molecular-level understanding of the OCS microhydrated cluster is crucial to unraveling the underlying relationship between its hydrolysis and corresponding solvation properties in the atmospheric condition.

From the molecular point of view, OCS is exciting because it has competitive H-bonding sites (O and S end), which can bind with water through $O_{OCS}\cdots H-O_W$ and $S_{OCS}\cdots H-O_W$ H-bonding fashion. Further, neutral OCS is linear, whereas anionic OCS is bent with negative adiabatic electron affinity, which means anionic OCS could only be produced as microhydrated clusters.[13,14] Chao et al. thoroughly investigated the mechanism of neutral OCS hydrolysis using quantum chemical methods and observed that the C═S bond is more prone to being attacked by the nucleophilic addition of water than the C═O bond.[15] Although the presence of $S_{OCS}\cdots O_W$, $O_{OCS}\cdots O_W$, and $C_{OCS}\cdots O_W$ interactions were previously reported between the neutral OCS and water molecules in the microhydrated clusters,[16] the origin, type of such interactions, and their impact on the hydration behavior remain grossly overlooked. However, in sharp contrast,

Received: November 1, 2022
Revised: March 8, 2023

we previously observed that water molecule binds with the anionic OCS moiety only through H-bonding interactions in their microhydrated clusters.[17,18]

Therefore, this article reports comprehensive theoretical analyses of the microhydrated neutral OCS molecule using the ab initio quantum chemical calculation, wherein the existence of several $S_{OCS}\cdots O_W$, $O_{OCS}\cdots O_W$, and $C_{OCS}\cdots O_W$ types of weak noncovalent interactions between water and the neutral OCS molecule are revealed. The effect of such interactions on the structure, energetics, and vibrational property up to OCS pentahydrates are discussed and compared with those of the anionic OCS microhydrates. The origin of such noncovalent interactions is also discussed using MESP, atoms in molecules (AIM), and NBO analyses. The present study thus reports a unique perspective on the impact of weak noncovalent interaction on the hydration behavior of neutral OCS molecules, which has not been elucidated before.

2. COMPUTATIONAL METHODS

2.1. Ab-Initio Quantum Chemical Calculation. All the electronic structure calculations of the different sizes of the microhydrated clusters of neutral OCS molecules were carried out using the Møller−Plesset perturbation theory of second-order (MP2) and aug-cc-pVDZ basis set using the Gaussian 16 quantum chemistry program.[19] The MP2 level of theory combined with the aug-cc-pVDZ basis set was found to reproduce experimental microwave rotational constant for the microhydrated clusters of the sulfur-containing compounds with sufficient accuracy, suggesting that this level of theory is suitable for investigating sulfur-water system.[20] Numerous guess structures were generated for the optimization based on the different H-bonding sites of OCS for various monohydrated complexes. For the OCS dihydrated complex, the guess structures were generated following the bottom-up approach, where the most stable (minimum energy) structure of the monohydrated complex was considered, and another water was added at different binding sites. The same approach was followed for the higher-order clusters of OCS and water molecules. The frozen core approximation and "very tight" convergence criteria were employed in the optimization. The harmonic frequency calculations were performed for all the optimized structures to ensure that the structures were at local minima.

The complexation energy (ΔE_{Comp}) of the mono to pentahydrated OCS complexes was calculated using the eq 1, where the zero-point vibrational energy (ZPVE) and basis-set superposition error (BSSE) corrected total energy of OCS and water were subtracted from the ZPVE, and BSSE corrected total energy of the complex.[17,18] Therefore, ΔE_{Comp} measures the total energy released due to the complexation of neutral OCS with water accounting for both solute−solvent and solvent−solvent interaction. Further, the ZPVE and BSSE corrected incremental association energy (ΔE_{IA}) was calculated according to eq 2, where the energy of the most stable complex and energy of the water monomer was subtracted from the next higher-order complexes.[17,18] Hence, ΔE_{IA} essentially measures the stabilization energy due to successive addition of water to the previous size microhydrated clusters and therefore highlights the solute−solvent interaction only; in other words, it reflects whether adding another water to the most stable cluster would directly benefit the solvation of the solute.

$$\Delta E_{Comp} = E^{OPT}_{OCS-(H_2O)_n} - E^{OPT}_{OCS} - nE^{OPT}_{H_2O} \quad (1)$$

$$\Delta E_{IA} = E^{OPT}_{OCS-(H_2O)_n} - E^{MS,OPT}_{OCS-(H_2O)_{n-1}} - E^{OPT}_{H_2O} \quad (2)$$

Relative population $[P_R(j)]$ of different conformers of the same size of the OCS hydrated clusters have been calculated using eq 3 with respect to the least stable (highest energy) conformation

$$P_R(j) = \frac{e^{-\Delta E_j/RT}}{\sum_{j=1}^{N} e^{-\Delta E_j/RT}} \quad (3)$$

Here ΔE_j accounts for the ZPVE and BSSE corrected stabilization energy of a particular conformer, and T is 298 K. Furthermore, the weighted average complexation and incremental association energies (ΔE_{WA}) for a particular cluster size were computed using the eq 4 where ΔE_j and corresponding relative population $[P_R(j)]$ were being used as follows.

$$\Delta E_{WA} = \sum_{j=1}^{N} P_R(j) \times \Delta E_j \quad (4)$$

2.2. Molecular Electrostatic Potential (MESP) Surfaces. The electrostatic potential mapped on the molecular surfaces (MESP) of neutral OCS microhydrates for the two minimum energy (most stable) structures for each cluster size were generated at the MP2/aug-cc-pVDZ level of theory from the previously optimized checkpoint file using the total SCF density at a selected isosurface value (0.001 au) and electrostatic potential of the molecule using Multiwfn program[21] and the construction of the MESP surfaces were performed using VMD.[22] The MESP, $\Phi(r)$ at point r, is defined based on Coulomb's law as follows[23]

$$\Phi(r) = \sum_A \frac{Z_A}{|R_A - r|} - \int \frac{\rho(r')}{|r' - r|} dr' \quad (5)$$

Here, Z_A is the charge of the nucleus at R_A, and $\rho(r)$ is the electron density. The $\Phi(r)$ accounts for both the contribution of nuclei and electrons. The positive $\Phi(r)$ represents a larger contribution of nuclei and, therefore, electrophilic sites on the molecular surface, whereas the negative $\Phi(r)$ corresponds to a greater contribution of electrons and hence represents a nucleophilic site on the surface. The MESP, therefore, can be regarded as the interaction energy between the molecules' charge distribution and a positive unit charge placed at r (in kcal/mol) and is extremely helpful in understanding various types of interactions.[24,25]

2.3. Atoms in Molecules (AIM) Analyses. AIM analyses[26−35] based on the topological analyses of electron density were performed on the optimized wave function of the microhydrated OCS clusters to characterize various noncovalent interactions. A molecular density map was generated for all the complexes using AIM software.[36] The electron density $[\rho(r)]$ and Laplacian of electron density $[\nabla^2\rho(r), L(r)]$ at each critical point connecting two nuclei known as a bond critical point (BCP) were computed. The presence of a (3, −1) type BCP in which the curvature of electron density in the direction of the line connecting two nuclei participated in the bonding is positive, while simultaneously the curvature in the two perpendicular directions to the bond path is negative, confirms the nonbonding interaction between two nuclei. However, only those BCPs have been considered for the noncovalent interaction in the OCS microhydrated clusters where $\rho(r)$ and $L(r)$ values are higher than 0.002 and 0.02 au, respectively.[34,37]

https://doi.org/10.1021/acs.jpca.2c07670
J. Phys. Chem. A XXXX, XXX, XXX−XXX

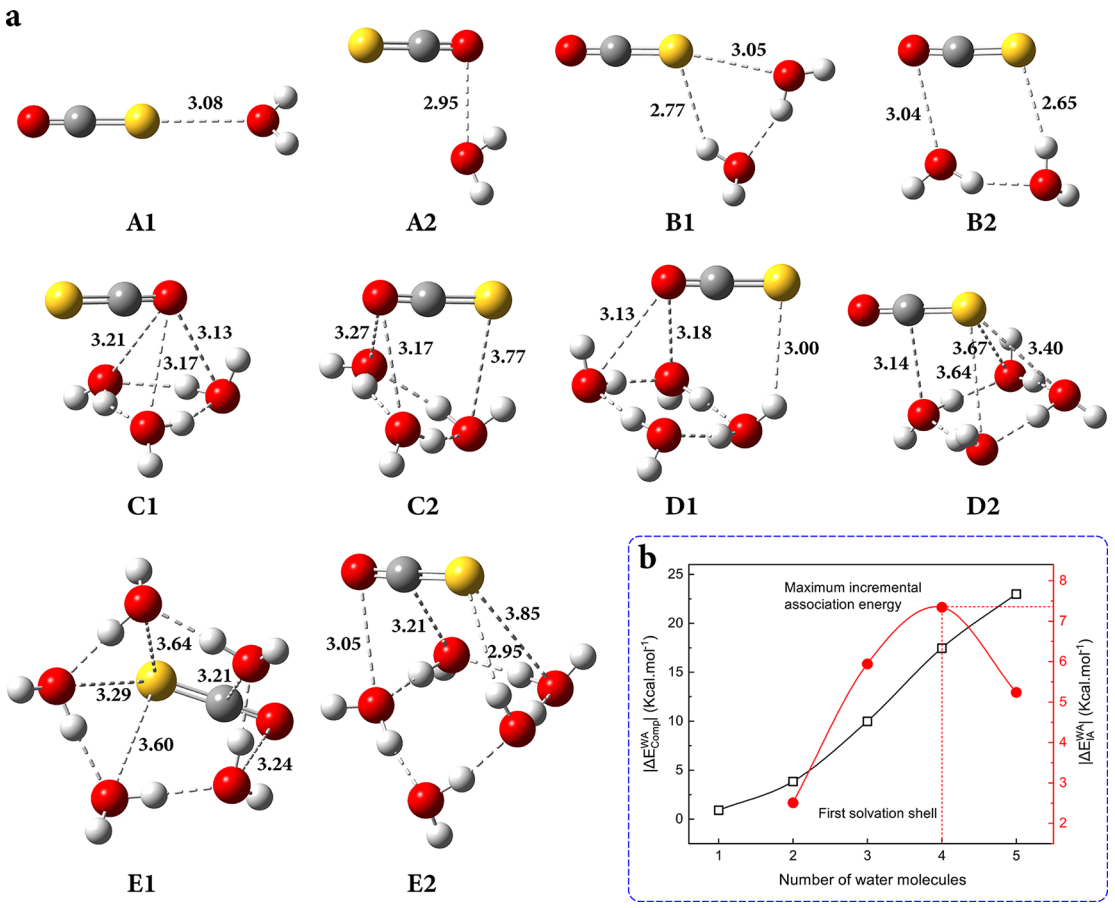

Figure 1. First two most stable (minimum energy) OCS microhydrates $[OCS\cdots(H_2O)_{n=1-5}]$ for each cluster size calculated at the MP2/aug-cc-pVDZ level of theory (a). The bond distances are in Å. The ZPVE and BSSE corrected weighted-average complexation energy $[|\Delta E^{WA}_{Comp}|]$ and incremental association energy $[|\Delta E^{WA}_{IA}|]$ of the OCS microhydrates (b). The signs of $|\Delta E^{WA}_{Comp}|$ and $|\Delta E^{WA}_{IA}|$ are negative for each cluster size.

Further, the sign of $L(r)$ can demonstrate the nature of the bonding interaction. The $L(r) > 0$ represents the depletion of the electronic charge locally in a particular region of space where the kinetic energy contribution of electron density is greater than the potential energy representing the H-bonding, ionic bonds, the van der Waals interactions, or other types of noncovalent interactions. In contrast, $\nabla^2\rho(r) < 0$ suggests a covalent bond where the electronic charge gets concentrated locally between two nuclei. Further, the amount of covalent character of chemical interactions can also be obtained from the electronic energy density $H(r)$, which reflects the interplay between the kinetic and potential energy density of the electron at the BCP according to eq 6

$$H(r) = G(r) + V(r) \tag{6}$$

The sign of $H(r)$ indicates whether the accumulation of charge at a given point r leads to either stabilizing $[H(r) < 0]$ or destabilizing $[H(r) > 0]$ effect. Further, the bond energy $E(r)$ can be calculated using eq 7

$$E(r) = \frac{V(r)}{2} \tag{7}$$

Finally, the nature of the bonding interaction between two nuclei can be obtained from the ratio $\left|\frac{G(r)}{V(r)}\right|$. The ratio $\left|\frac{G(r)}{V(r)}\right| > 1$ suggests that the interaction is noncovalent type; whereas $0.5 < \left|\frac{G(r)}{V(r)}\right| < 1$ indicates that the interaction is partly a covalent type.[38,39] Additionally, (i) the weak interactions can be characterized from both positive $\nabla^2\rho(r)$ and $H(r)$ values and (ii) moderately strong interactions from the positive $\nabla^2\rho(r)$ and negative $H(r)$ values, whereas (iii) strong interactions are seen from both negative $\nabla^2\rho(r)$ and $H(r)$ values.[40] Furthermore, the bond ellipticity, $\varepsilon(r)$, at the BCP was also calculated according to eq 8, which is the measure of the anisotropy of electron density at the BCP and can reflect the π- or σ-bond character of a chemical interaction between two nuclei

$$\varepsilon(r) = \frac{\lambda_1}{\lambda_2} - 1 \tag{8}$$

Here, λ's are the negative vectors associated with the Hessian of $\rho(r)$ at the respective CP and $\lambda_2 \leq \lambda_1$. The greater the value of $\varepsilon(r)$ more is the accumulation of electron density at the perpendicular axes at the BCP along the bond path connecting two nuclei, the greater is the π-bond character.

2.4. Natural Bond Orbital (NBO) Analyses. Finally, NBO analyses were performed on the optimized structures of each complex using the built-in NBO3.1 functionality of the Gaussian 16 package to calculate the charges on different atoms and understand the origin of such noncovalent interactions in the neutral OCS microhydrates.[41] The relevant charge shift and the associated energies (kcal·mol^{-1}) for different clusters were also calculated using NBO analyses.

https://doi.org/10.1021/acs.jpca.2c07670
J. Phys. Chem. A XXXX, XXX, XXX−XXX

3. RESULTS AND DISCUSSION

3.1. Structures and Energetics. Different OCS microhydrated clusters up to pentahydrate were optimized using the MP2/aug-cc-pVDZ level of theory following the bottom-up approach, the details of which are mentioned in the methodology section. The first two of the most stable (minimum energy) structures for each microhydrated OCS cluster size are shown in Figure 1a (see Supporting Note 1 for all the optimized structures). The ZPVE and BSSE corrected complexation ($|\Delta E_{Comp}|$) and incremental association energies ($|\Delta E_{IA}|$) of neutral OCS microhydrates of different sizes estimated using eq 1 are shown in Table S1. The sign of $|\Delta E_{Comp}|$ and $|\Delta E_{IA}|$ for all the OCS microhydrates $[OCS\cdots(H_2O)_{n=1-5}]$ presented in this work are negative, which means stabilization due to complexation with water molecules. In the most stable monohydrate A1, surprisingly, the water interacts with the OCS molecule through $S_{OCS}\cdots O_W$ noncovalent interaction with a bonding distance of 3.08 Å and $|\Delta E_{Comp}|$ of 1.17 kcal·mol^{-1}. In A2, the water molecule interacts with OCS through $O_{OCS}\cdots O_W$ interaction with 2.95 Å distance and $|\Delta E_{Comp}|$ of 0.65 kcal·mol^{-1}. The relative population of A1 and A2 are 51% and 27%, respectively. Interestingly, in A3 (see Figure S1), where water interacts with OCS through a typical $O_{OCS}\cdots H-O_W$ H-bond is the least stable and accounts for only ∼22% population.

A similar noncovalent interaction, which has a significant stabilizing effect, is also present in the OCS dihydrates. In B1, there is one $O_{OCS}\cdots H-O_W$ type interwater hydrogen bond (IWHB) along with $S_{OCS}\cdots H-O_W$ H-bond and a $S_{OCS}\cdots O_W$ noncovalent interaction where the bonding distance is found to be 2.77 and 3.05 Å respectively with the $|\Delta E_{Comp}|$ of 4.04 kcal·mol^{-1}. In B2, one $O_{OCS}\cdots O_W$ interaction between water and OCS moiety with a 3.04 Å bonding distance can be observed where another water molecule interacts through the sulfur end of OCS through the $S_{OCS}\cdots H-O_W$ H-bond, having 2.65 Å bonding distance and 3.49 kcal·mol^{-1} of $|\Delta E_{Comp}|$.

C1 is the most stable conformation among OCS trihydrates where water interacts with the OCS similarly through $O_{OCS}\cdots O_W$ noncovalent interaction with the bonding distance ranging from 3.13 to 3.21 Å along with the IWHBs among water molecules. C2 also exhibits a similar trend where there are IWHBs among water molecules; however, two water molecules interact with the oxygen end of OCS through an $O_{OCS}\cdots O_W$ interaction, whereas another water interacts with the sulfur end through a $S_{OCS}\cdots O_W$ interaction with a distance ranging from 3.17 to 3.77 Å. The $|\Delta E_{Comp}|$ values of C1 and C2 are 10.11 and 9.92 kcal·mol^{-1}, respectively. In the case of C3 also, the water network grows at the sulfur end through $S_{OCS}\cdots O_W$ interaction and IWHBs among water molecules. Surprisingly, C4, where $S_{OCS}\cdots H-O_W$ H-bond is present along with a new $C_{OCS}\cdots O_W$ noncovalent interaction, and C5, where $O_{OCS}\cdots H-O_W$ and $S_{OCS}\cdots H-O_W$ H-bonds and $C_{OCS}\cdots O_W$ noncovalent interaction are present (see Figure S1), are among the least stable OCS trihydrates.

OCS tetrahydrates show a total of seven conformations where the most stable structure, D1, has two $O_{OCS}\cdots O_W$ interactions (3.13 and 3.18 Å) along with $S_{OCS}\cdots H-O_W$ H-bond between water molecules and OCS alongside IWHBs among water molecules accounting for the vast stabilization of 17.74 kcal·mol^{-1} and 35% of the population among the tetrahydrates. In D2, there are three $S_{OCS}\cdots O_W$ interactions along with one $C_{OCS}\cdots O_W$ interaction between OCS and water molecules, which accounts for the huge 17.67 kcal·mol^{-1} stabilization and around 29% of the population among the OCS tetrahydrates. In D3, four $O_{OCS}\cdots O_W$ interactions exist whereas, in D4, two $C_{OCS}\cdots O_W$ and two $S_{OCS}\cdots O_W$ interactions are present between water and OCS along with IWHBs between water molecules. Take note that D3 and D4 do not have a single $O_{OCS}\cdots H-O_W$/$S_{OCS}\cdots H-O_W$ type of H-bond but still account for the massive stabilization of 17.13 (D3) and 17.10 kcal·mol^{-1} (D4). D3 and D4 also correspond to around 16% and 13% of the population among the OCS tetrahydrates. In other clusters (D5, D6, and D7), mainly $O_{OCS}\cdots O_W$ and $C_{OCS}\cdots O_W$ interactions are predominant, along with some $S_{OCS}\cdots H-O_W$ H-bond between OCS and water molecules along with IWHBs.

Further, the most stable OCS pentahydrate, E1, consists of three $S_{OCS}\cdots O_W$, one $C_{OCS}\cdots O_W$, and one $O_{OCS}\cdots O_W$ interaction between OCS and water molecules along with IWHBs. E1 accounts for a whopping 65% population among pentahydrates and 23.48 kcal·mol^{-1} stabilization energy. In E2, there is one of each $C_{OCS}\cdots O_W$, $O_{OCS}\cdots O_W$, and $S_{OCS}\cdots O_W$ noncovalent interaction and one $S_{OCS}\cdots H-O_W$ H-bonding between OCS and water molecules along with IWHBs accounting for the 10% population with a huge 22.54 kcal·mol^{-1} of $|\Delta E_{Comp}|$. In other conformations, as well, the $S_{OCS}\cdots O_W$, $O_{OCS}\cdots O_W$, and $C_{OCS}\cdots O_W$ noncovalent interactions between OCS and water molecules remain the predominant mode of interaction. It can be observed that the number of noncovalent interactions increases with the increase of the OCS microhydrated cluster size.

It can be summarized that neutral OCS microhydrates are stabilized predominantly by the noncovalent $S_{OCS}\cdots O_W$, $O_{OCS}\cdots O_W$, and $C_{OCS}\cdots O_W$ interactions between the OCS and water molecules, whereas the $O_{OCS}\cdots H-O_W$/$S_{OCS}\cdots H-O_W$ type of H-bonds has minimal impact on their stabilization. To confirm that the present result does not arise from the method-dependent biases, first, optimized geometries were perturbed to ensure that the initial geometries only have typical H-bonds ($O_{OCS}\cdots H-O_W$/$S_{OCS}\cdots H-O_W$) between water molecules and the OCS moiety before optimizing again at the same level of theory. However, those attempts remained unsuccessful, and the same optimized geometries were obtained. Second, the most stable conformers (A1, B1, C1, D1, E1) were optimized using MPWB1K, a hybrid meta-GGA (generalized gradient approximation) functional best known for accurately describing weak noncovalent and charge transfer interactions[42] coupled with 6-311++G** basis set to make sure that the $S_{OCS}\cdots O_W$/$O_{OCS}\cdots O_W$/$C_{OCS}\cdots O_W$ type noncovalent interactions do not arise only in a particular method or basis set. The optimized geometries at the MPWB1K/6-311++G** level of theory (A1*, B1*, C1*, D1*, E1*), are presented in Figure S2 of the Supporting Note 2, which shows that all the optimized geometries are precisely the same as the most stable conformations obtained at the MP2/aug-cc-pVDZ level of theory except D1*. In D1*, there is only one $O_{OCS}\cdots O_W$ interaction and another $O_{OCS}\cdots H-O_W$ H-bond compared to two $O_{OCS}\cdots O_W$ noncovalent interactions and one $S_{OCS}\cdots H-O_W$ H-bond in D1. Nonetheless, this different method, coupled with another basis set, demonstrates that the microhydrated OCS complex is predominantly stabilized by the noncovalent interactions instead of the typical H-bonds between OCS and water molecules.

Previously, we also reported the minimum energy (most stable) structure of the neutral OCS microhydrates up to six water clusters optimized at the MP2/6-311++G(D,P) level of theory.[17] The optimized minimum energy structures A1, C1, D1, and E1 at the MP2/aug-cc-pVDZ level of theory reported in this study are identical with the corresponding structures from

https://doi.org/10.1021/acs.jpca.2c07670
J. Phys. Chem. A XXXX, XXX, XXX−XXX

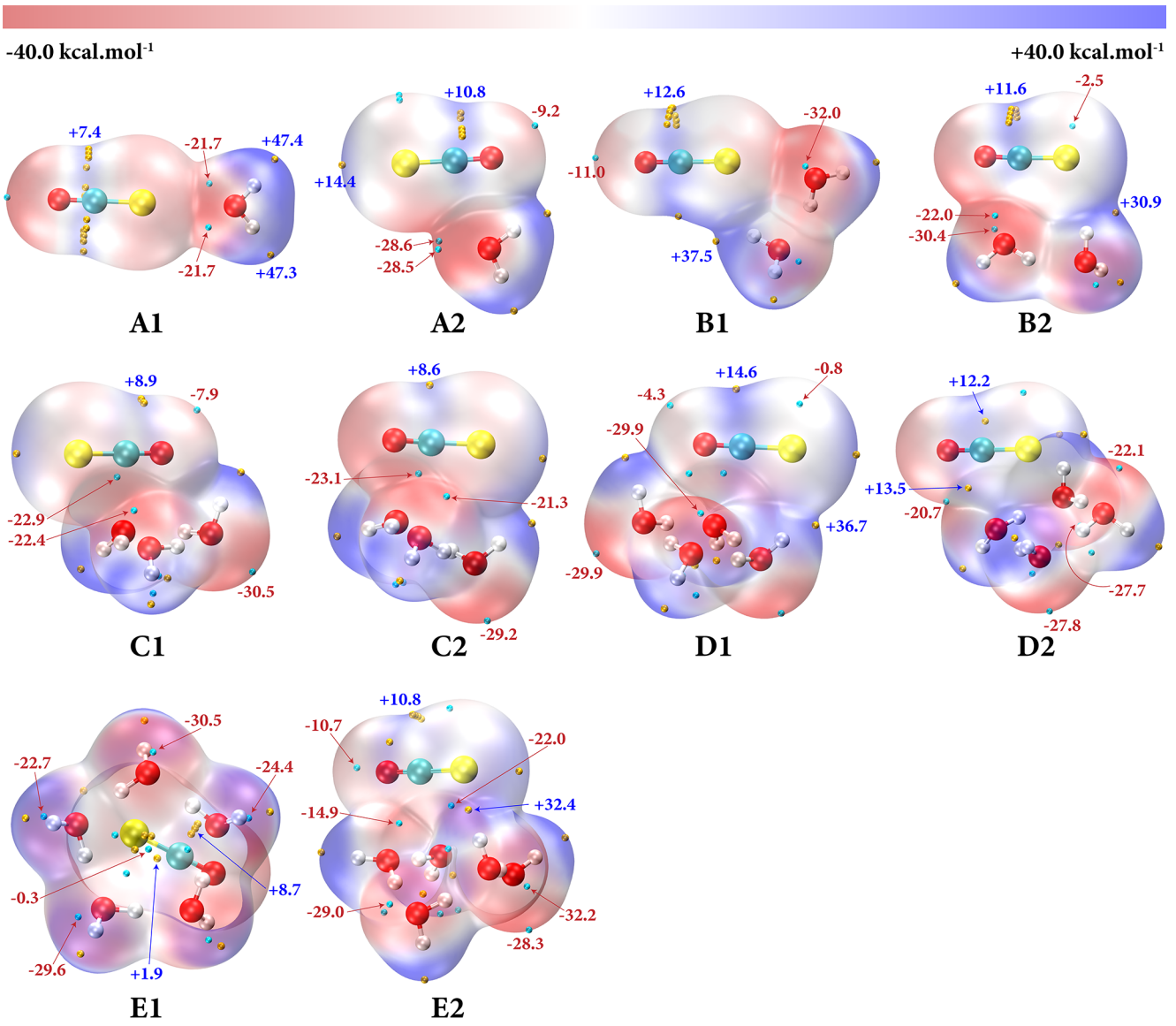

Figure 2. Molecular electrostatic potential (MESP) surfaces of the two least energy (most stable) neutral OCS microhydrate for each cluster size. The molecular surface of OCS···$(H_2O)_{n=1-5}$ with red color represents the negative MESP values, whereas the blue color corresponds to positive MESP values, whereas the color bar of the MESP surfaces is presented on the top. The positive maxima (small sphere of dark yellow) and negative minima (small sphere of dark cyan) on the MESP surfaces are shown. The MESP values are presented in kcal·mol^{-1}. The big red, yellow, dark cyan, and white spheres, respectively, represent an oxygen atom, sulfur atom, carbon atom, and hydrogen atom.

the previous study. However, the most stable OCS dihydrate reported in the previous study does not match either B1 or B2, which might be because that structure does not represent a local minimum structure and is probably higher in energy than either B1 or B2 and is not a stable complex when optimized using "very tight" convergence criteria. Furthermore, the dashed lines shown in Figure 1a of the previous work[17] representing the H-bonding interaction between the OCS moiety and water molecules are also grossly misleading as we now understand that not the typical O_{OCS}···H−O_W and S_{OCS}···H−O_W H-bonds but predominantly the S_{OCS}···O_W, O_{OCS}···O_W, and C_{OCS}···O_W type of weak noncovalent interaction is responsible for the complexation. Another interesting fact that can be observed from Figure 1 of the previous work is that the OH bond of water molecules largely points away from the neutral OCS, whereas it orients toward the anionic OCS moiety, which is one of the motivations that has led to this more in-depth analysis of the neutral OCS microhydrates.

To understand the energetics of these neutral OCS microhydrates, the ZPVE and BSSE corrected weighted average complexation ($|\Delta E^{WA}_{Comp}|$) and incremental association energy ($|\Delta E^{WA}_{IA}|$) for each cluster size were calculated, which are shown in Figure 1b (see Table S1 for details). The $|\Delta E^{WA}_{Comp}|$ increases from 0.91 kcal·mol^{-1} in the OCS monohydrates to 23.0 kcal·mol^{-1} for the OCS pentahydrates. The linear fitting of the $|\Delta E^{WA}_{Comp}|$ with respect to the cluster size (number of water molecules) indicates that each water adds roughly 5.78 kcal·mol^{-1} stabilization energy to the microhydrated cluster. However, the $|\Delta E^{WA}_{Comp}|$ accounts for both solute−solvent and solvent−solvent interactions. Therefore, $|\Delta E^{WA}_{IA}|$ was computed, reflecting the energy released due to the OCS−water interaction. The $|\Delta E^{WA}_{IA}|$ of the neutral OCS microhydrates increase up to the tetrahydrates, and it decreases subsequently

https://doi.org/10.1021/acs.jpca.2c07670
J. Phys. Chem. A XXXX, XXX, XXX−XXX

for the pentahydrates, showing a maximum for tetrahydrated cluster which indicates that the first solvation shell of neutral OCS consists of four water molecules similar to the previously studied anionic OCS microhydrates.[17,18] The addition of further water molecules does not directly participate in bonding with OCS moiety; instead, it adds up to the IWHBs and increases the $|\Delta E_{Comp}^{WA}|$.

3.2. Molecular Electrostatic Potential (MESP) Surfaces. The MESP surfaces, along with relevant maxima and minima of the two most stable (least energy) OCS microhydrates for each cluster size, are presented in Figure 2, where red color represents the negative MESP (in kcal·mol^{-1}), and the blue color indicates the positive MESP. Furthermore, the positive maxima at the MESP surface reflect the attenuation of the electronic charge and hence are attracted by the electron-rich site, whereas the negative minima are attracted by the positive or extremely low electronegative sites. The maxima and minima at the MESP surface are depicted as small spheres of respective dark cyan and dark yellow color in Figure 2.

In A1, two minima (−21.7 kcal·mol^{-1}) at the MESP surface can be observed around the oxygen atom of the water molecule, whereas a number of maxima around the C atom along the perpendicular plane of the OCS moiety; however, there are no minima at the MESP surface of the S atom. Therefore, the strong negative electrostatic potential of the water O atom interacts with the very weak negative potential of the S atom of the OCS moiety. Similarly, in A2, the O atom of the water molecule with strong negative potential with two minima at the MESP surface (−28.5, −28.6 kcal·mol^{-1}) interacts with the relatively weak negative potential of the O atom of OCS from a perpendicular direction with a surface minimum of −9.2 kcal·mol^{-1}. In B1 and B2, minima of respectively −32.0 and −22.0, 30.4 kcal·mol^{-1} at the MESP surface can be observed around the water O atom, which with its strong negative potential, interacts with the very weak negative potential of respectively S and O atoms of the OCS moiety. Also, there is the electrostatic attraction between the large positive MESP (+37.5 and 30.9 kcal·mol^{-1}) of water O−H H atom and very weak negative potential of S atom in respectively B1 and B2. These interactions between two sites having a positive and negative electrostatic potential is a typical H-bonding interaction. Also, a ring of positive potential around the C atom of OCS moiety in those two clusters can be noticed. In other higher-order clusters, as well, the strong negative potential of the water O atom (see the minima at the MESP surface) interacts with the S and O atoms of OCS having weakly negative potential or C atom of OCS having weakly positive potential predominantly from a perpendicular orientation with respect to the OCS moiety. In all these complexes, the MESP values of the water oxygen atom are very large negative values compared to that in the O or S end of the OCS moiety.

Apparently, these unfavorable interactions in the neutral OCS microhydrates between two sites with the same negative potential but different magnitude are impossible to stabilize the cluster solely from an electrostatic standpoint. However, counterintuitively, these interactions produce an energetically stable complex ($\Delta E_{Comp} = -ve$), and the least energy, neutral OCS monohydrate A1 was experimentally observed.[43] These noncovalent interactions between two atoms having the same sign of MESP were reported before as counterintuitive interactions.[23,24,44] The feasibility of these interactions was explained using the Feynman−Hellman theorem, which says that the force that holds nuclei and electrons of a molecule together is classically Coulombic in nature.[23] Further, it has been demonstrated that the electrostatic interaction between two ground-state unperturbed molecules occurs in tandem with the polarization of their electron cloud because, as they approach, the electric field of the molecule alters the electronic charge distribution/polarizability of the other, and hence those two events should not be considered separately. Instead, polarization is an integral part of the Coulombic interaction.[44] Furthermore, the polarization of the electron density of a molecule by the incoming dipole is always inherently stabilizing. Therefore, for weak noncovalent interactions between the same negative MESP sites, as can be observed for neutral OCS microhydrates, the destabilization caused by the unfavorable electrostatic repulsion between weak and strong negative potential can be outweighed by the stabilizing contribution of strong polarization of the electron density by the electric field of the other molecule. Further, to unravel more insights into the nature of these interactions, the topology of the electron density was analyzed using AIM analyses, discussed in the following section.

3.3. AIM Analyses. AIM analyses were performed on the wave functions for the optimized OCS microhydrates to understand the origin and characterize these noncovalent interactions ($S_{OCS}\cdots O_W/O_{OCS}\cdots O_W/C_{OCS}\cdots O_W$) between the neutral OCS and water molecules. The molecular density map (contour plots) of the first two most stable complexes for each cluster size was generated using the AIM analyses and shown in Figure 2 (see Figure S3 for all the clusters). The topological parameters corresponding to noncovalent interactions, i.e., electron density [$\rho(r)$, ρ], Laplacian of electron density [$\nabla^2\rho(r)$, L], ellipticity [$\varepsilon(r)$, ε], bond energy [$E(r)$, E], total energy density [$H(r)$, H], and the modulus of the ratio of kinetic to potential energy density $\left[R = \frac{G(r)}{V(r)}\right]$ at the BCP and the bonding distance (r), along with the atomic charges obtained from the natural population analysis (NPA) for all the complexes, are tabulated in Table S2 of the Supporting Note 3. The presence of a (3, −1) BCP along with a positive ρ greater than 0.002 and an L greater than 0.02 is considered a noncovalent interaction between two interacting nuclei. Similarly, a (3, −1) ring critical point (RCP) and a positive L indicate a cyclic interaction.

In A1, there is a (3, −1) BCP between S and O atoms, and the corresponding values of L and ρ are, respectively, 0.034 and 0.009, which confirms that the sulfur atom of OCS moiety interacts with the O atom of the water molecule with a bond energy of 1.88 kcal·mol^{-1}. The optimized structure of A1 is identical to the experimentally obtained structure of Tatamitani and co-workers using microwave Fourier transform spectroscopy.[43] In A2, surprisingly, a BCP between the O of OCS and O of water with a positive L and ρ (0.009 and 0.038) can be observed with the corresponding bond energy of 2.51 kcal·mol^{-1}. In structure A3, a typical H-bond between O of OCS and H of water moiety can be found with the L and ρ, respectively, of 0.012 and 0.044 and a bond energy of 2.82 kcal·mol^{-1}. In all these OCS monohydrates, the positive L and H, along with the R > 1 at the BCP, suggest that these interactions are weak noncovalent types. Also, a comparison of the topological parameters of these interactions at the BCP (see Table S2) reveals that the $O_{OCS}\cdots O_W$ interaction with a relatively shorter bonding distance is slightly stronger than the $S_{OCS}\cdots O_W$ interaction in the OCS microhydrated cluster. The ε value for the $S_{OCS}\cdots O_W$ interaction in A1 is lower compared to the $O_{OCS}\cdots O_W$ interaction in A2, which reflects that the $S_{OCS}\cdots O_W$ interaction has more σ-bond character than the $O_{OCS}\cdots O_W$

https://doi.org/10.1021/acs.jpca.2c07670
J. Phys. Chem. A XXXX, XXX, XXX−XXX

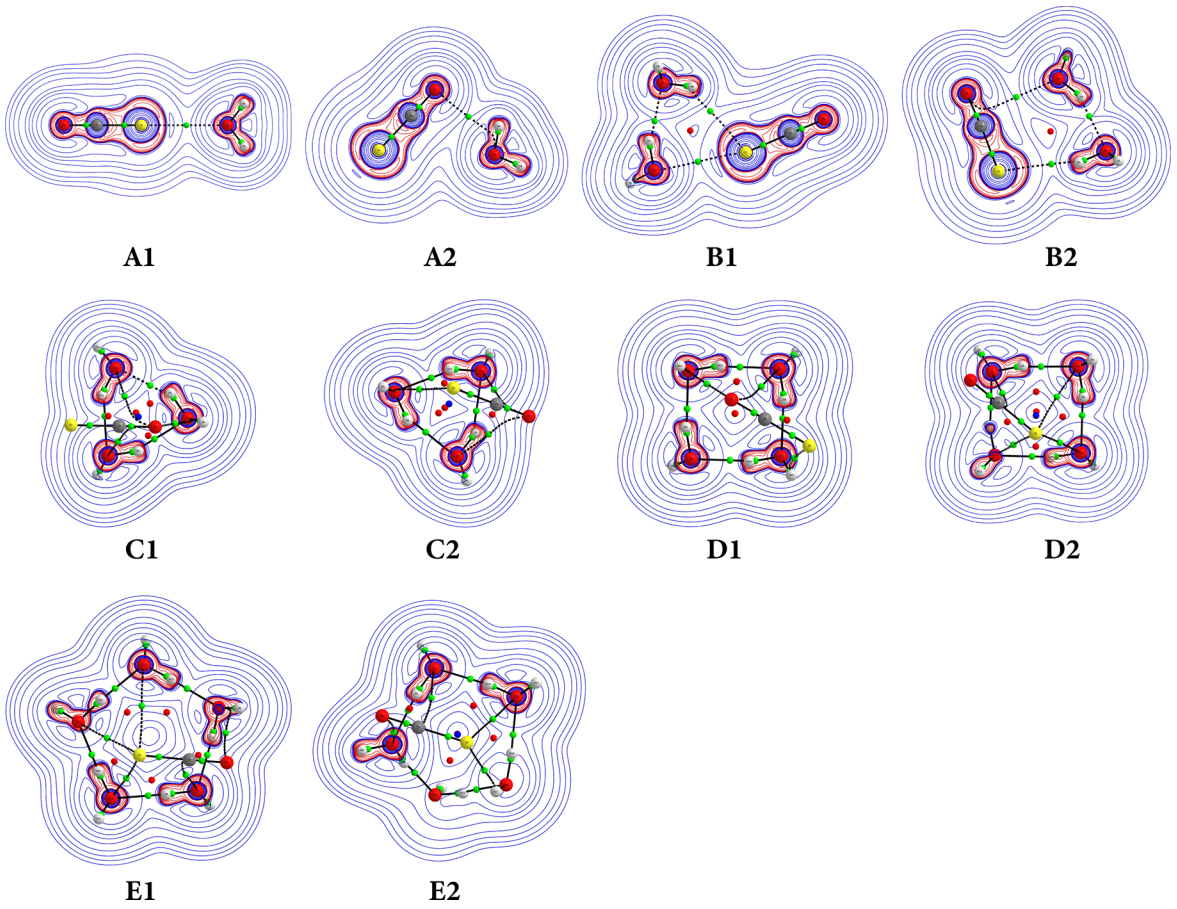

Figure 3. Electron density map of (a) monohydrates (A1−A2), (b) dihydrates (B1−B2), (c) trihydrates (C1−C2), (d) tetrahydrates (D1−D2), and (e) pentahydrates (E1−E2) of OCS molecule calculated at the MP2/aug-cc-pVDZ level of theory. The small green, red, and blue spheres signify the (3, −1) bond critical point (BCP), the (3, +1) ring critical point (RCP), and the (3, +3) cage critical point, respectively. The large red, gray, yellow, and white spheres represent oxygen, carbon, sulfur, and hydrogen, respectively. The black dashed curves show the possible bond paths between two interacting atoms.

interaction. In A3, ε is even less, showing a substantial σ-bond character for a typical H-bond.

In the OCS dihydrate B1, the L, ρ for the $S_{OCS}\cdots O_W$ interaction is 0.036, and 0.010 au, respectively, which confirms their existence. Additionally, there is a $S_{OCS}\cdots H-O_W$ type of H-bond between OCS and water with the L and ρ values respectively 0.008 and 0.024 au. However, interestingly, the E of the $S_{OCS}\cdots O_W$ interaction is higher (2.20 kcal·mol^{-1}) compared to the $S_{OCS}\cdots H-O_W$ H-bond (1.57 kcal·mol^{-1}), showing that the $S_{OCS}\cdots O_W$ interaction is marginally stronger than $S_{OCS}\cdots H-O_W$ H-bond. In both these cases, the ε values are close to zero (0.10, 0.05, respectively), indicating that both these interactions have a strong σ-bond character. Similarly, $O_{OCS}\cdots O_W$ interaction between the OCS moiety and water can be observed in B2 with the L and ρ values of 0.036, 0.008 respectively, along with the $S_{OCS}\cdots H-O_W$ H-bond with the L and ρ values of 0.010 and 0.026, respectively. The ε value of $O_{OCS}\cdots O_W$ interaction in B2 is 1.87, which suggests that this interaction has a substantial π-bond character, whereas the corresponding ε value of $S_{OCS}\cdots H-O_W$ H-bond is 0.03, indicating significant σ-bond character. However, both positive L, H values and $R > 1$ for all the interactions at the BCP in both B1 and B2 suggest that they are all weak noncovalent interactions.

Surprisingly, in the OCS trihydrate C1, there are three BCPs for the $O_{OCS}\cdots O_W$ interaction between OCS moiety and water molecules with L values of 0.029, 0.027, and 0.023 and the ρ values of 0.007, 0.006, and 0.005, respectively, with the corresponding E of 1.57, 1.26, and 1.26 kcal·mol^{-1}. The ε values of those interactions are 0.50, 3.77, and 5.16, respectively, indicating that the π-bond character of these interactions can vary considerably depending upon the mode of interaction between the OCS and water molecules. In C2, BCPs can be found for two $O_{OCS}\cdots O_W$ interactions and one $S_{OCS}\cdots O_W$ interaction between OCS and water molecule. The ε for the $S_{OCS}\cdots O_W$ interaction is 0.57 compared to 3.18 and 1.36 for the two $O_{OCS}\cdots O_W$ interactions, which suggests that $S_{OCS}\cdots O_W$ interaction has a greater σ-bond character than either of these $O_{OCS}\cdots O_W$ interactions. However, the bond energies of these interactions suggest that $O_{OCS}\cdots O_W$ interactions are stronger than the $S_{OCS}\cdots O_W$ interaction. In C3, L and ρ values confirm the presence of three $S_{OCS}\cdots O_W$ interactions with corresponding E ranging from 0.63 to 1.57 kcal·mol^{-1}. Relatively low ε values close to zero for all these interactions suggest a profound σ-bond character and isotropic electron density along the bond path. In the structures C4 and C5, interestingly, BCPs can be observed for the $C_{OCS}\cdots O_W$ interaction between OCS and water molecule, which has L and ρ values of 0.034, 0.008 and 0.038, 0.009 respectively, accompanying typical $O_{OCS}\cdots H-O_W$ and $S_{OCS}\cdots H-O_W$ H-bonds. In both cases, the ε values for the $C_{OCS}\cdots O_W$ interaction are considerable, respectively, 2.39 and 1.97, indicating significant anisotropy of the electron density along the perpendicular axis to the bond path connecting two nuclei.

https://doi.org/10.1021/acs.jpca.2c07670
J. Phys. Chem. A XXXX, XXX, XXX−XXX

Table 1. Total Electron Shift to OCS, Corresponding Total Stabilization Energy Due to Electron Transfer (from Water to OCS and OCS to Water, in kcal·mol^{-1}), the Principal Component (PC, in kcal·mol^{-1}), and the Participating Bonding (Donor) and Antibonding (Acceptor) Orbital in the Secondary Orbital Interaction[a]

comp	ΔQ_{CT}(OCS) × 10^{-3} (e)	$\lvert\Delta E_{CT}\rvert$	$\lvert\Delta E_{W\text{-}OCS}\rvert$	$\lvert\Delta E_{OCS\text{-}W}\rvert$	$\lvert\Delta E_{PC}\rvert$ (%)	D_{NBO}	A_{NBO}
A1	−3.00	2.42	2.05	0.37	1.67 (69.0)	LP(O_4)	BD*(C_2–S_3)
A2	−0.48	2.10	1.33	0.77	0.46 (21.9)	LP(O_4)	BD*(O_1–C_2)
B1	−0.71	4.83	2.23	2.60	1.80 (37.3)	LP(S_3)	BD*(O_7–H_9)
					1.53 (31.7)	LP(O_4)	BD*(C_2–S_3)
B2	2.87	6.38	2.06	4.32	3.16 (49.5)	LP(S_3)	BD*(O_4–H_5)
					0.99 (15.5)	LP(O_7)	BD*(O_1–C_2)
C1	−2.09	2.49	2.04	0.45	0.58 (23.3)	LP(O_7)	BD*(O_1–C_2)
					0.35 (14.1)	LP(O_{10})	BD*(O_1–C_2)
					0.14 (5.60)	BD(O_{10}-H_{11})	BD*(O_1–C_2)
C2	−1.65	2.45	1.77	0.68	0.66 (26.9)	LP(O_{10})	BD*(O_1–C_2)
					0.38 (15.5)	LP(O_7)	BD*(O_1–C_2)
					0.23 (9.40)	LP(S_3)	BD*(O_4–H_5)
D1	−0.07	1.75	0.72	1.03	0.67 (38.3)	LP(S_3)	BD*(O_{13}–H_{15})
					0.34 (19.4)	LP(O_7)	BD*(O_1–C_2)
D2	−1.37	2.39	1.21	1.18	0.68 (28.5)	LP(O_7)	BD*(O_1–C_2)
					0.21 (8.8)	BD*(O_1–C_2)	RY*(O_7)
					0.17 (7.1)	LP(S_3)	RY*(O_7)
					0.14 (5.9)	BD (C_2–S_3)	RY*(O_7)
					0.13 (5.4)	LP (S_3)	BD*(O_{13}–H_{15})
E1	−1.60	2.93	1.59	1.34	0.45 (15.4)	LP(O_7)	BD*(O_1–C_2)
					0.31 (10.6)	LP(O_4)	BD*(O_1–C_2)
					0.27 (9.2)	LP(S_3)	BD*(O_{10}-H_{11})
					0.21 (7.2)	BD(O_1–C_2)	BD*(O_4–H_5)
					0.19 (6.5)	LP(O_{10})	BD*(C_2–S_3)
					0.16 (5.5)	BD*(O_1–C_2)	RY*(O_7)
E2	−1.23	3.81	1.97	1.84	0.88 (23.1)	LP (S_3)	BD*(O_{16}–H_{17})
					0.78 (20.5)	LP(O_7)	BD*(O_1–C_2)
					0.35 (9.2)	BD*(O_1–C_2)	RY*(O_7)
					0.35 (9.2)	LP(O_4)	BD*(O_1–C_2)

[a]The signs of the stabilization energies $\lvert\Delta E_{CT}\rvert$, $\lvert\Delta E_{W\text{-}OCS}\rvert$, $\lvert\Delta E_{OCS\text{-}W}\rvert$, $\lvert\Delta E_{PC}\rvert$ are negative.

Though these interactions offer significant stability to the OCS trihydrated clusters, the positive L, H, and $R > 1$ values for all the interactions at the BCP suggest that these interactions are also weak noncovalent types.

A similar trend can be observed in the tetrahydrate and pentahydrate OCS clusters as well. In D1 (Figure 3), BCPs can be found for two $O_{OCS}\cdots O_W$ interactions between the OCS and water molecules along with one $S_{OCS}\cdots H{-}O_W$ type H-bond. One of the $O_{OCS}\cdots O_W$ interactions have a large ε of 1.76, suggesting a greater π-bond character than other interactions. In D2, BCPs can be observed for one $C_{OCS}\cdots O_W$ and three $S_{OCS}\cdots O_W$ interactions between OCS moiety and water molecules where the E can vary significantly from 0.63 to 1.26 kcal·mol^{-1}. Furthermore, in D3, BCPs are present for four $O_{OCS}\cdots O_W$ type interactions where the bond energy varies from 0.63 to 1.57 kcal·mol^{-1} and ε from 0.05 to 1.88, reflecting a large π -bond character for some interactions. In other tetrahydrates, several BCPs can be found for $O_{OCS}\cdots O_W$, $S_{OCS}\cdots O_W$, and $C_{OCS}\cdots O_W$ type interactions with a varied range of bond strengths and anisotropy of electron density (see Table S2 for E and ε). In the OCS pentahydrated clusters, the number of BCPs observed for the $O_{OCS}\cdots O_W$, $S_{OCS}\cdots O_W$, and $C_{OCS}\cdots O_W$ interactions between the OCS moiety and water molecules increases substantially. The L and ρ values corresponding to these interactions are large positive values ranging from 0.006 to 0.035 and 0.003 to 0.015, respectively, whereas E varies from 0.63 to 3.15 kcal·mol^{-1} (see Supporting Note 3), suggesting that the strength of these interactions could differ significantly based on the structure of the complex. In these OCS tetrahydrates and pentahydrates, R values vary from 1.0 to 2.0, which, coupled with positive L and ρ values, suggest that these interactions are extremely weak noncovalent types. Interestingly, the ε of these interactions also varies substantially from ∼0.1 to ∼3.5, reflecting that these interactions could have significantly different anisotropy of the electron density along the bond path based on the mode of interactions.

The present study thus unravels significant differences between the microhydrated clusters of metastable anionic OCS, which we have reported previously,[17,18] and the neutral OCS in terms of their structural organization and the type of interactions between the OCS and water molecules. The anionic OCS microhydrates are stabilized by typical $O_{OCS}\cdots H{-}O_W$/$S_{OCS}\cdots H{-}O_W$ type of H-bonds between the OCS moiety and water molecules along with the IWHBs; however, no such noncovalent interactions were observed. In contrast, for neutral OCS, an overwhelming population of $S_{OCS}\cdots O_W$/$O_{OCS}\cdots O_W$/$C_{OCS}\cdots O_W$ noncovalent interactions is present in the OCS microhydrates. Furthermore, it can be observed that for the anionic OCS microhydrates, the water H-bond network grows on the surface of the OCS molecule in a particular direction covering the whole OCS moiety. In contrast, the water network grows primarily around one atom (either S/O) or two atoms (O, C or C, S) depending upon the structure itself in different sizes of the neutral OCS microhydrates. These facts hint that the

https://doi.org/10.1021/acs.jpca.2c07670
J. Phys. Chem. A XXXX, XXX, XXX−XXX

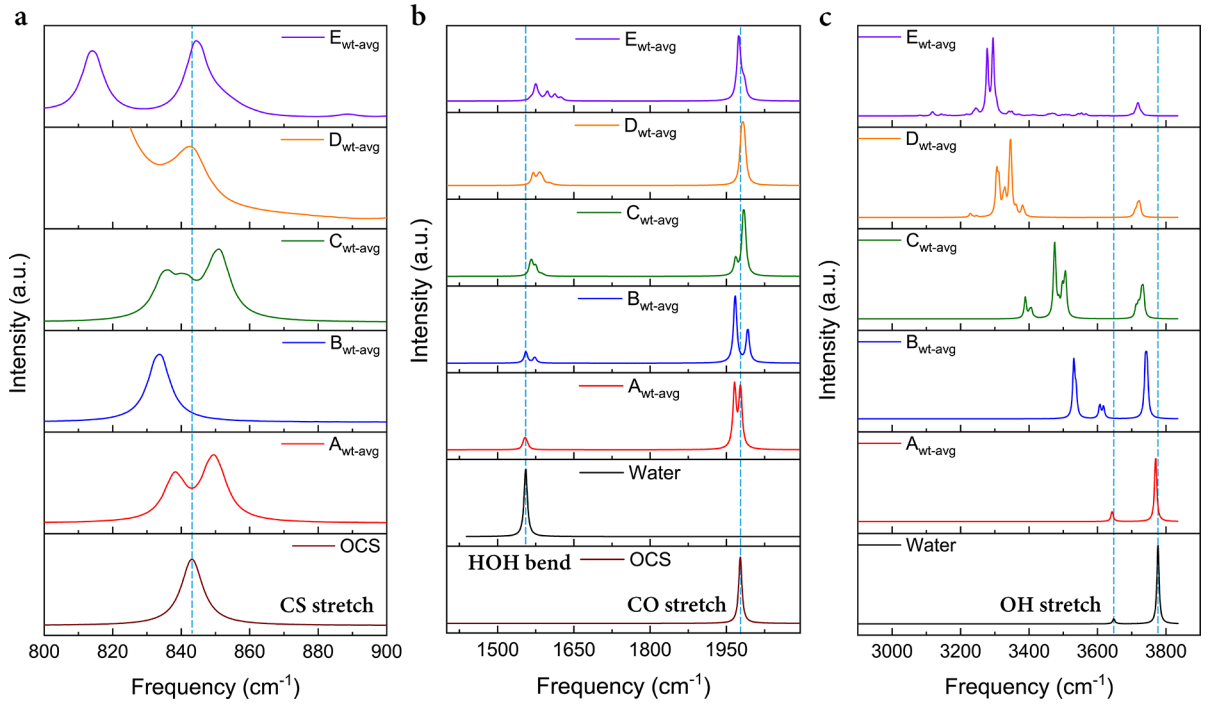

Figure 4. Weighted average IR spectra of the OCS microhydrates for each cluster size.

water molecules interact with the OCS in an entirely different fashion in their respective clusters of neutral and anionic forms. Hence, it can be hypothesized that the anionic OCS microhydrates try to maximize the interaction between OCS moiety and water through a double H-bond between water and the OCS moiety ($O_{OCS}\cdots H-O_W$, $S_{OCS}\cdots H-O_W$) and the rest of the water network grows on top of it in a particular direction through IWHBs. In contrast to that in the neutral OCS microhydrates, as the system's overall electron density is significantly low, there is less probability of having strong electrostatic interactions between OCS and water molecules. Therefore, the system maximizes the IWHBs between water molecules first, and then the whole water cluster interacts with the S/O end of the OCS moiety to maximize the number of noncovalent ($S_{OCS}\cdots O_W$/$O_{OCS}\cdots O_W$/$C_{OCS}\cdots O_W$) interactions within the clusters. However, it is difficult to understand why in the case of neutral OCS, the corresponding microhydrated cluster exclusively prefers these unique noncovalent interactions over the typical H-bonds between OCS moiety and water molecules. We shall return to this point later in this article.

3.4. NBO Analyses. To understand the origin of the weak noncovalent interaction and the electron donor−acceptor property of the interacting atoms, the NBO analyses were performed. The total charge density shift along with the energy transfer from OCS to water and vice versa and their corresponding principal components are listed in Table 1 for the first two most stable OCS microhydrates for each cluster size and all the optimized clusters in Table S3 of Supporting Note 5. Figure S5 shows the donor and acceptor NBOs involved in the principal component of the energy transfer (kcal·mol^{-1}) between OCS and water molecules in the neutral OCS microhydrated clusters.

It can be observed that, for A1, the total charge shifted from water to OCS is 0.003e, suggesting that in A1, water behaves as an electron donor to OCS. The principal component of this transfer comes from the electron shifts from the nonbonding orbital of oxygen [$LP(O_4)$] of water to the antibonding orbital of the C−S bond [$BD^*(C_2-S_3)$] of the OCS corresponding to the 1.67 kcal·mol^{-1} stabilization. In A2, the electron is donated to the $BD^*(O_1-C_2)$ of the OCS molecule from the $LP(O_4)$ of water which provides 0.46 kcal·mol^{-1} of stabilization (Figure S5).

Similarly, in B1, the net charge donated from water to OCS is about 0.00071e, suggesting that water again acts as an electron donor to OCS moiety. The electron is donated from the $LP(S_3)$ of OCS to the $BD^*(O_7-H_9)$ of water as well as from the $LP(O_4)$ of water to the $BD^*(C_2-S_3)$ of OCS, accounting for the 1.80 and 1.53 kcal·mol^{-1} of stabilization, respectively. In contrast to that, the OCS molecule acts as an electron donor and water as an acceptor as there is a net electron shift of 0.00287e from OCS to water in B2. Therefore, in both B1 and B2, we found that electrons are donated both by OCS to water and water to OCS, which correlates well with their cyclic structure (Figures 1a and 3). Similarly, in the higher-order cluster as well, the electron is shifted both from OCS to water and vice versa, primarily from the $LP(O_1)$ or $LP(S_3)$ of OCS to the $BD^*(O-H)$ of water as well as the lone pair of oxygen of water to the $BD^*(O_1-C_2)$ or $BD^*(C_2-S_3)$ of OCS which primarily accounts for the stabilization of the OCS microhydrates.

Further, it can be observed that electrons can be shifted from $BD(O_{10}-H_{11})$ of water to the $BD^*(O_1-C_2)$ of OCS as in the case of C1, accounting for the 0.14 kcal·mol^{-1} of stabilization along with the electron transfer from the water oxygen lone pair to the $BD^*(O_1-C_2)$. Surprisingly in the case of C3 (Table S3, Supporting Note 5), electron transfer takes place from the $BD(O_{10}-H_{12})$ of water to the higher energy Rydberg state, $RY^*(S_3)$ of OCS, and $BD(C_2-S_3)$ of OCS to $RY^*(O_{10})$ of water which corresponds to 0.18 and 0.13 kcal·mol^{-1} of energy. This charge shifts from the bonding orbital to the virtual state due to secondary orbital interactions involving OCS and water molecules becoming more feasible as cluster size increases. For example, D2, which is a cyclic structure, shows some

https://doi.org/10.1021/acs.jpca.2c07670
J. Phys. Chem. A XXXX, XXX, XXX−XXX

secondary orbital interaction where electron transfer takes place from both LP(S_3), BD(C_2−S_3), and BD*(O_1−C_2) of OCS to the RY*(O_7) of water accounting for the 0.21, 0.17, and 0.14 kcal·mol^{-1} stabilization, respectively. There is also electron transfer from the nonbonding to the antibonding orbital from the OCS to water and vice versa, corresponding to a net charge shift of 0.00137e from water to OCS moiety.

For the pentahydrate, E1, electron transfer mainly takes place from the LP(O_7) of water to the BD*(O_1−C_2) of OCS, BD(O_1−C_2) of OCS to BD*(O_4−H_5), and BD*(O_1−C_2) of OCS to RY*(O_7) of water representing 0.45, 0.21, and 0.16 kcal·mol^{-1} of stabilization energy, respectively. The net charge shift from the water to OCS is 0.00160e, indicating that overall, water acts as the electron donor to the OCS. In the case of E2, we observe the electron transfer from the BD*(O_1−C_2) of OCS to the RY*(O_7) of water, accounting for 0.35 kcal·mol^{-1} stabilization along with other interactions like the electron transfer from the LP(S_3) of OCS to the BD*(O_{16}−H_{17}) or O atom of water [LP(O_4), LP(O_7)] or C═O bond of OCS [BD*(O_1−C_2)]. Therefore, in the microhydrated clusters, the electron transfer from water to OCS and vice versa are highly feasible, sometimes involving high-energy states. This observation helps to understand the origins of the weak noncovalent interactions between neutral OCS and water molecules, accounting for huge stabilization when the typical H-bonding is not the preferred mode of interaction. This study further unravels that where the electrostatic interaction is unfavorable, as in the case of neutral OCS microhydrates, charge shift occurs mainly from the LP(O) of water to the BD*(C═S) of OCS, altering the charge distribution of the complex considerably making the C═S bond more vulnerable against the nucleophilic substitution in a hydrolysis reaction than the C═O bond.[15]

3.5. Vibrational Property. The harmonic frequencies of individual clusters were calculated at the MP2/aug-cc-pVDZ level of theory listed in Table S4 of the Supporting Note 6 to understand how the charge-shifted interactions impact the vibrational properties of the OCS microhydrates. The scaling factor was calculated to be 0.959. Furthermore, the weighted average IR spectrum was computed using the relative population of different conformations (see Table S1 of Supporting Note 1) for each size of the microhydrated cluster, (Figure 4). Both water symmetric and asymmetric stretch undergoes substantial redshift upon successive addition of water which signifies a cyclic, cooperative H-bonded network of water molecules. However, OH symmetric stretch gets shifted significantly more than OH asymmetric stretch with the increase of water molecules in the cluster.

Furthermore, it can be observed that the HOH bending mode gets blueshifted upon successive addition of water from the OCS mono- to pentahydrate. Though there is a slight shift in the CO and CS stretching frequency, the spectral broadening from the small (monohydrate) to large size cluster (pentahydrate) is substantial. This result is in good agreement with both the MESP surface and NBO analyses, which show that water acts as an electron donor to OCS moiety, whereas frequency analysis shows that water bending mode predominantly acts as electron donor mode for the electron transfer from water to OCS moiety.

Though the harmonic frequencies are very sensitive to the water H-bond of the OCS hydrated clusters, the frequency calculation of the C═S and C═O bond of the respective hydrated clusters particularly are not so sensitive to the local environment (see Table S4). More specifically, it can be observed that the change in C═O or C═S stretching frequencies is abrupt and could not be correlated well with the observed electron shift. Hence, the anharmonic frequency calculation of the OCS hydrated complexes was performed at the MP2/aug-cc-pVDZ level of theory up to OCS tetrahydrated complexes (first solvation shell) where the frequencies of the C═S, C═O, and O−H symmetric and asymmetric stretch mode are presented in Table S5 for the first two most stable complexes. Anharmonic frequencies of OH symmetric and asymmetric stretch mode show that water molecule undergoes redshift, indicating that OCS-water interaction is overwhelmed by the substantial contribution from the cyclic IWHBs among water molecules for all the optimized clusters. In the case of A1, both C═S and C═O stretch undergoes redshift of 3.8 cm^{-1} and 10.6 cm$^{-1,}$ respectively, along with the water symmetric and antisymmetric stretch mode, which is, in fact, counterintuitive because there is a net charge transfer of 0.003 au from water to OCS moiety. However, in A2, the overall charge transfer occurs from the water LP(O_4) to the BD*(O1−C2) of OCS, which correlates well with the redshift of the C═O stretch (0.4 cm^{-1}). However, the C═S stretch undergoes a blue shift, indicating that it can sometimes act as an electron donor. In B2, C═O gets red-shifted, corroborating that OCS acts as the electron donor to water.

However, in higher-order clusters (B1, C1−C2, and D1−D2), the C═S stretch mode undergoes a redshift along with the blueshift in the C═O stretching mode, which corroborates well with the observed electron shift pathway revealed by the NBO analyses. The blueshift of the C═O stretch band may also arise from Pauli's repulsive forces due to geometric constraints outweighing the stabilizing effects of attractive electrostatic forces.[45] Nevertheless, because, we primarily observe a net charge shift from water to OCS, this factor is less probable. Therefore, in combination with the NBO analyses, it can be inferred that the σ-type of orbital interaction leads to the redshift of the stretching frequency, whereas the π-type of interaction among the bonding and higher energy states leads to the blueshift in general. Further, the weighted average IR has shown that the water bending mode is increasingly blueshifted upon successive addition of water (see Figure 4); it signifies that the water bending mode is predominantly perturbed due to the net charge shift from water molecule to the C═S moiety of the OCS.

4. CONCLUSION

The microhydrated OCS clusters up to pentahydrate are systematically investigated using ab initio quantum chemical calculations, MESP surfaces, AIM, and NBO analyses to understand their structure, energetics, and vibrational properties. The $|\Delta E^{WA}_{Comp}|$ shows that adding each water molecule to the OCS microhydrates adds ∼5.8 kcal·mol^{-1} stabilization to the system. Additionally, the $|\Delta E^{WA}_{IA}|$ shows that the first solvation shell of microhydrated OCS consists of four water molecules. Further, MESP, in tandem with AIM analyses, reveals that water predominantly solvates OCS molecules through unique weak noncovalent $C_{OCS}\cdots O_W$, $S_{OCS}\cdots O_W$, and $O_{OCS}\cdots O_W$ interaction and not with the typical H-bonds. The NBO analyses show that water molecule primarily acts as electron donor, especially in the higher-order clusters where electrons can be directly donated from the LP(O) of water molecules to the BD*(C−S) or shifted via BD*(C−O) of OCS moiety. Furthermore, the anharmonic frequency analyses show that this charge transfer has a profound impact on the water bending mode as well as C═O and C═S stretching mode. In OCS tri- and tetrahydrates, water bending

https://doi.org/10.1021/acs.jpca.2c07670
J. Phys. Chem. A XXXX, XXX, XXX−XXX

and C═O stretch modes undergo blueshifts, whereas the C═S stretch mode undergoes a redshift, which corroborates well with the electron transfer pathway observed from NBO analyses. Therefore, the present study unravels the surprising stability of the microhydrated neutral OCS molecule through charge-shifted weak noncovalent interactions. We hope the present study offers a unique perspective to understanding the structure, stability, and hydrolysis process of OCS in atmospheric conditions.

■ ASSOCIATED CONTENT

Supporting Information

The Supporting Information is available free of charge at https://pubs.acs.org/doi/10.1021/acs.jpca.2c07670.

All the structures of the optimized microhydrated clusters at MP2/aug-cc-pVDZ level of theory, the structure of the most stable conformations of the microhydrated neutral OCS clusters optimized at MPWB1K/6-311++G** level of theory, AIM and NBO analyses along with harmonic and anharmonic frequencies of C═O and C═S, and water stretching and bending modes (PDF)

■ AUTHOR INFORMATION

Corresponding Author

Saptarsi Mondal − *School of Chemical Sciences, Indian Association for the Cultivation of Sciences, Kolkata 700032, India;* Present Address: Center for Molecular Spectroscopy and Dynamics, Institute of Basic Sciences (IBS), Seoul 02841, Republic of Korea; orcid.org/0000-0003-1140-9322; Email: sapta.chem.iitb@gmail.com

Complete contact information is available at: https://pubs.acs.org/10.1021/acs.jpca.2c07670

Notes

The author declares no competing financial interest.

■ ACKNOWLEDGMENTS

I extend my sincere gratitude to Prof. Prashant Chandra Singh of the Indian Association for the Cultivation of Science (IACS), Kolkata, for the generous support and many discussions. I thank IACS for the financial support and the supercomputing facility at IACS for the computational support. I also want to thank Dr. Tanay Debnath for his many helpful suggestions.

■ REFERENCES

(1) Modiri Gharehveran, M.; Hain, E.; Blaney, L.; Shah, A. D. Influence of dissolved organic matter on carbonyl sulfide and carbon disulfide formation from cysteine during sunlight photolysis. *Environ. Sci.: Process. Impacts* **2020**, *22* (9), 1852−1864.

(2) Hattori, S.; Kamezaki, K.; Yoshida, N. Constraining the atmospheric OCS budget from sulfur isotopes. *Proc. Natl. Acad. Sci. U.S.A.* **2020**, *117* (34), 20447−20452.

(3) Rastogi, B.; Berkelhammer, M.; Wharton, S.; Whelan, M. E.; Meinzer, F. C.; Noone, D.; Still, C. J. Ecosystem fluxes of carbonyl sulfide in an old-growth forest: temporal dynamics and responses to diffuse radiation and heat waves. *Biogeosciences* **2018**, *15* (23), 7127−7139.

(4) Bunk, R.; Yi, Z.; Behrendt, T.; Wu, D.; Andreae, M. O.; Kesselmeier, J. Carbonyl sulfide (OCS) exchange between soils and the atmosphere affected by soil moisture and compensation points. *Biogeosciences Discuss.* **2018**, *2018*, 1−29.

(5) Commane, R.; Meredith, L. K.; Baker, I. T.; Berry, J. A.; Munger, J. W.; Montzka, S. A.; Templer, P. H.; Juice, S. M.; Zahniser, M. S.; Wofsy, S. C. Seasonal fluxes of carbonyl sulfide in a midlatitude forest. *Proc. Natl. Acad. Sci. U.S.A.* **2015**, *112* (46), 14162−14167.

(6) Maseyk, K.; Berry, J. A.; Billesbach, D.; Campbell, J. E.; Torn, M. S.; Zahniser, M.; Seibt, U. Sources and sinks of carbonyl sulfide in an agricultural field in the Southern Great Plains. *Proc. Natl. Acad. Sci. U.S.A.* **2014**, *111* (25), 9064−9069.

(7) Brühl, C.; Lelieveld, J.; Crutzen, P. J.; Tost, H. The role of carbonyl sulphide as a source of stratospheric sulphate aerosol and its impact on climate. *Atmos. Chem. Phys.* **2012**, *12* (3), 1239−1253.

(8) Brugnoli, E.; Calfapietra, C. Carbonyl sulfide: a new tool for understanding the response of the land biosphere to climate change. *New Phytol.* **2010**, *186* (4), 783−785.

(9) Mohammadi, A. H.; Richon, D. CLATHRATE HYDRATE PHASE EQUILIBRIA FOR CARBONYL SULFIDE, HYDROGEN SULFIDE, ETHYLENE, OR PROPANE + WATER SYSTEM BELOW WATER FREEZING POINT. *Chem. Eng. Commun.* **2013**, *200* (12), 1635−1644.

(10) Vaida, V.; Headrick, J. E. Physicochemical Properties of Hydrated Complexes in the Earth's Atmosphere. *J. Phys. Chem. A* **2000**, *104* (23), 5401−5412.

(11) Zhao, S.; Yi, H.; Tang, X.; Jiang, S.; Gao, F.; Zhang, B.; Zuo, Y.; Wang, Z. The Hydrolysis of Carbonyl Sulfide at Low Temperature: A Review. *Scientific World J.* **2013**, *2013*, 1−8.

(12) Luther III, G. W. Kinetics of the Reactions of Water, Hydroxide Ion and Sulfide Species with CO2, OCS and CS2: Frontier Molecular Orbital Considerations. *Aquat. Geochem.* **2004**, *10* (1/2), 81−97.

(13) Surber, E.; Sanov, A. Photoelectron imaging spectroscopy of molecular and cluster anions: CS2− and OCS−(H2O)1,2. *J. Chem. Phys.* **2002**, *116* (14), 5921−5924.

(14) Surber, E.; Ananthavel, S. P.; Sanov, A. Nonexistent electron affinity of OCS and the stabilization of carbonyl sulfide anions by gas phase hydration. *J. Chem. Phys.* **2002**, *116* (5), 1920−1929.

(15) Deng, C.; Li, Q.-G.; Ren, Y.; Wong, N.-B.; Chu, S.-Y.; Zhu, H.-J. A comprehensive theoretical study on the hydrolysis of carbonyl sulfide in the neutral water. *J. Comput. Chem.* **2008**, *29* (3), 466−480.

(16) Hartt, G. M.; Shields, G. C.; Kirschner, K. N. Hydration of OCS with One to Four Water Molecules in Atmospheric and Laboratory Conditions. *J. Phys. Chem. A* **2008**, *112* (19), 4490−4495.

(17) Mondal, S.; Teja, A. U.; Singh, P. C. Theoretical Study on the Microhydration of Atmospherically Important Carbonyl Sulfide in Its Neutral and Anionic Forms: Bridging the Gap between the Bulk and Finite Size Microhydrated Cluster. *J. Phys. Chem. A* **2015**, *119* (15), 3644−3652.

(18) Mondal, S.; Teja, A. U.; Singh, P. C. Effect of microhydration on the atmospherically important metastable carbonyl sulfide anion: Structure, energetic, and infrared study. *Int. J. Quantum Chem.* **2015**, *115* (12), 785−795.

(19) *Gaussian 16*, Rev. C.01; Gaussian: Wallingford, CT, 2016.

(20) Kirschner, K. N.; Hartt, G. M.; Evans, T. M.; Shields, G. C. In search of CS2(H2O)n = 1−4 clusters. *J. Chem. Phys.* **2007**, *126* (15), 154320.

(21) Lu, T.; Chen, F. Multiwfn: A multifunctional wavefunction analyzer. *J. Comput. Chem.* **2012**, *33* (5), 580−592.

(22) Humphrey, W.; Dalke, A.; Schulten, K. VMD: Visual molecular dynamics. *J. Mol. Graph.* **1996**, *14* (1), 33−38.

(23) Politzer, P.; Murray, J. S.; Clark, T. Mathematical modeling and physical reality in noncovalent interactions. *J. Mol. Model.* **2015**, *21* (3), 52.

(24) Murray, J. S.; Politzer, P. Can Counter-Intuitive Halogen Bonding Be Coulombic? *ChemPhysChem* **2021**, *22* (12), 1201−1207.

(25) Liu, L.; Miao, L.; Li, L.; Li, F.; Lu, Y.; Shang, Z.; Chen, J. Molecular Electrostatic Potential: A New Tool to Predict the Lithiation Process of Organic Battery Materials. *J. Phys. Chem. Lett.* **2018**, *9* (13), 3573−3579.

(26) Bader, R. F. W. The density in density functional theory. *Comp. Theor. Chem.* **2010**, *943* (1−3), 2−18.

(27) Bader, R. F. W. Bond Paths Are Not Chemical Bonds. *J. Phys. Chem. A* **2009**, *113* (38), 10391−10396.

(28) Bader, R. F. W. Confined Atoms Treated as Open Quantum Systems. *Adv. Quantum Chem.* **2009**, *57*, 285−318.
(29) Matta, C. F.; Bader, R. F. W. An Experimentalist's Reply to "What Is an Atom in a Molecule? *J. Phys. Chem. A* **2006**, *110* (19), 6365−6371.
(30) Bader, R. F. W. Comment on the Comparative Use of the Electron Density and Its Laplacian. *Chem. Eur. J.* **2006**, *12* (30), 7769−7772.
(31) Bader, R. F. W.; Fang, D.-C. Properties of Atoms in Molecules: Caged Atoms and the Ehrenfest Force. *J. Chem. Theory Comput.* **2005**, *1* (3), 403−414.
(32) Hernández-Trujillo, J.; Bader, R. F. W. Properties of Atoms in Molecules: Atoms Forming Molecules. *J. Phys. Chem. A* **2000**, *104* (8), 1779−1794.
(33) Bader, R. F. W.; Bayles, D. Properties of Atoms in Molecules: Group Additivity. *J. Phys. Chem. A* **2000**, *104* (23), 5579−5589.
(34) Popelier, P. L. A. Characterization of a Dihydrogen Bond on the Basis of the Electron Density. *J. Phys. Chem. A* **1998**, *102* (10), 1873−1878.
(35) Bader, R. F. W. A quantum theory of molecular structure and its applications. *Chem. Rev.* **1991**, *91* (5), 893−928.
(36) Biegler-König, F. *J. Comput. Chem.* **2001**, *22* (5), 545−559.
(37) Koch, U.; Popelier, P. L. A. Characterization of C-H-O Hydrogen Bonds on the Basis of the Charge Density. *J. Phys. Chem.* **1995**, *99* (24), 9747−9754.
(38) Abboud, J. L. M.; Mo, O.; de Paz, J. L. G.; Yanez, M.; Esseffar, M.; Bouab, W.; El-Mouhtadi, M.; Mokhlisse, R.; Ballesteros, E. Thiocarbonyl versus carbonyl compounds: A comparison of intrinsic reactivities. *J. Am. Chem. Soc.* **1993**, *115* (26), 12468−12476.
(39) Hocquet, A. Intramolecular hydrogen bonding in 2′-deoxyribonucleosides: an AIM topological study of the electronic density. *Phys. Chem. Chem. Phys.* **2001**, *3* (15), 3192−3199.
(40) Rozas, I.; Alkorta, I.; Elguero, J. Behavior of Ylides Containing N, O, and C Atoms as Hydrogen Bond Acceptors. *J. Am. Chem. Soc.* **2000**, *122* (45), 11154−11161.
(41) Reed, A. E.; Curtiss, L. A.; Weinhold, F. Intermolecular interactions from a natural bond orbital, donor-acceptor viewpoint. *Chem. Rev.* **1988**, *88* (6), 899−926.
(42) Zhao, Y.; Truhlar, D. G. Benchmark Databases for Nonbonded Interactions and Their Use To Test Density Functional Theory. *J. Chem. Theory Comput.* **2005**, *1* (3), 415−432.
(43) Tatamitani, Y.; Ogata, T. Microwave Fourier transform spectrum of the water-carbonyl sulfide complex. *J. Chem. Phys.* **2004**, *121* (20), 9885−9890.
(44) Clark, T.; Murray, J. S.; Politzer, P. A perspective on quantum mechanics and chemical concepts in describing noncovalent interactions. *Phys. Chem. Chem. Phys.* **2018**, *20* (48), 30076−30082.
(45) Li, X.; Liu, L.; Schlegel, H. B. On the Physical Origin of Blue-Shifted Hydrogen Bonds. *J. Am. Chem. Soc.* **2002**, *124* (32), 9639−9647.

https://doi.org/10.1021/acs.jpca.2c07670
J. Phys. Chem. A XXXX, XXX, XXX−XXX